Dating carbonaceous matter in archean cherts by electron paramagnetic resonance

Mathilde Bourbin, Didier Gourier, Laurent Binet, Yann Le Du, Sylvie Derenne, Francès Westall, Barbara Kremer, Pascale Gautret

ASTROBIOLOGY
Volume 13, Number 2, 2013

DOI: 10.1089/ast.2012.0855

Dating Carbonaceous Matter in Archean Cherts by Electron Paramagnetic Resonance

M. Bourbin,[1] D. Gourier,[2] S. Derenne,[1] L. Binet,[2] Y. Le Du,[2] F. Westall,[3] B. Kremer,[4] and P. Gautret[5]

Abstract

Ancient geological materials are likely to be contaminated through geological times. Thus, establishing the syngeneity of the organic matter embedded in a mineral matrix is a crucial step in the study of very ancient rocks. This is particularly the case for Archean siliceous sedimentary rocks (cherts), which record the earliest traces of life. We used electron paramagnetic resonance (EPR) for assessing the syngeneity of organic matter in cherts that have a metamorphic grade no higher than *greenschist.* A correlation between the age of Precambrian samples and the shape of their EPR signal was established and statistically tested. As thermal treatments impact organic matter maturity, the effect of temperature on this syngeneity proxy was studied; cyanobacteria were submitted to cumulative short thermal treatment at high temperatures followed by an analysis of their EPR parameters. The resulting carbonaceous matter showed an evolution similar to that of a thermally treated young chert. Furthermore, the possible effect of metamorphism, which is a longer thermal event at lower temperatures, was ruled out for cherts older than 2 Gyr, based on the study of Silurian cherts of the same age and same precursors but various metamorphic grades. We determined that even the most metamorphosed sample did not exhibit the lineshape of an Archean sample. In the hope of detecting organic contamination in Archean cherts, a "contamination-like" mixture was prepared and studied by EPR. It resulted that the lineshape analysis alone does not allow contamination detection and that it must be performed along with cumulative thermal treatments. Such treatments were applied to three Archean chert samples, making dating of their carbonaceous matter possible. We concluded that EPR is a powerful tool to study primitive organic matter and could be used in further exobiology studies on low-metamorphic grade samples (from Mars for example). Key Words: Kerogen—Sedimentary rocks—Contamination—Spectroscopy—Archean. Astrobiology 13, 151–162.

1. Introduction

The most ancient traces of life, as old as about 3.5 Gyr, are recorded in silicified sediments (cherts). Although the mineral matrix can be accurately dated by using the U-Pb isotopes, for instance (Faure, 1986), dating the organic matter within the rocks is more problematic as fractions of it may be more recent than the mineral matrix due to contamination processes such as weathering, hydrothermalism, colonization by endolithic microorganisms, or anthropogenic contamination (Hoering, 1967; Roedder, 1981; Campbell, 1982; Knoll *et al.,* 1986; Westall and Folk, 2003). This can lead to incorrect conclusions about the presence of fossilized traces of life. The possibility of contamination results in a need for independent syngeneity markers, that is, proxies proving that the organic matter does not result from any contamination process and is of the same age as the mineral matrix.

Our study began by selecting samples and using clues for syngeneity, both at the macroscopic and the microscopic scales (Hoering, 1966). Because of contamination issues, correct interpretation of the microscopic remains of microorganisms requires undertaking small-scale stratigraphic mapping and multiple samplings at each studied locality (Buick, 1990). Rigorous procedures for collecting and preparing samples must be observed. Optical microscopy study of petrographic thin sections has to be used as the primary source of context information and, eventually, paleontological information if the microfossils are large enough to be observed by this method. At the microscopic scale, syngeneity clues are given

[1]Biogéochimie et Ecologie des Milieux Continentaux, UMR CNRS 7618, Université Pierre et Marie Curie, Paris, France.
[2]Laboratoire de Chimie de la Matière Condensée de Paris, Ecole Nationale Supérieure de Chimie de Paris, UMR CNRS 7574, Paris, France.
[3]Centre de Biophysique Moléculaire, UPR CNRS 4301, Orléans, France.
[4]Institute of Paleobiology, Polish Academy of Sciences, Warszawa, Poland.
[5]CNRS/INSU, ISTO, UMR 7327, Orléans, France.

by morphological criteria, reflecting the close relationship between the organic matter and the mineral matrix. Those criteria include (i) the presence of minerals embedded in the organic matter or organic matter embedded in a mineral matrix; (ii) the presence of later veins cutting the whole structure; (iii) the diversity of microbial colonies and biofilms; (iv) the distribution of the structures in the sample; (v) the variability in the level of preservation and silicification of the structures; (vi) the maturity of the organic matter (Westall *et al.,* 2006; Westall, 2011; Westall and Cavalazzi, 2011). However, younger microorganisms inhabiting cracks in the host rock may be present and may also become fossilized (Westall and Folk, 2003). They present all aforementioned macroscopic and microscopic properties, except that they are not embedded within minerals—they occur along cracks and mineral grain boundaries—and are thus sometimes difficult to differentiate from older endogenous structures. Finally, great care must be given to the interpretation of the local context and habitability of the environment in which the host rock was formed to determine whether the environment was conducive to the kind of organisms found in it (Westall, 2008).

Once the sample is selected, based on the aforementioned macroscopic and microscopic observations, syngeneity must be assessed with complementary techniques. Nanoscale secondary ion mass spectrometry (NanoSIMS) silicon and oxygen mapping was proposed to be a good syngeneity marker. This technique illustrates the intimate relationship of silica with organic matter, which probably reflects the permineralization process of biological remains (Oehler *et al.,* 2009). However, isotopic values obtained on Archean samples by NanoSIMS have large error bars (Robert *et al.,* 2008). Moreover, if care is not taken during the analytical procedure (*e.g.,* by using rigorous cleaning methods and/or stepped combustion), isotopic values in very ancient rocks may reflect younger contamination rather than older endogenous signal, as for cherts from the Isua Greenstone Belt in Greenland (Westall and Folk, 2003).

Electron paramagnetic resonance (EPR) is a nondestructive and non-invasive technique that has long been used for dating the mineral matrices in cherts and flints younger than ~1 Myr by monitoring the line intensity of irradiation-induced defects (Robins *et al.,* 1978; Porat and Schwarcz, 1991; Skinner, 2000). Paramagnetic defects, in the form of organic radicals, are also always present in carbonaceous material. They have been detected with high sensitivity in coals by pioneering EPR studies (Uebersfeld and Erb, 1956). These types of radicals were therefore used for the characterization of a wide range of carbonaceous materials, ranging from coals (Retcofsky *et al.,* 1968; Mrozowski, 1988a, 1988b) to cherts (Skrzypczak-Bonduelle *et al.,* 2008) or meteorites (Binet *et al.,* 2002, 2004; Gourier *et al.,* 2008; Delpoux *et al.,* 2011). The EPR signal of kerogen has the form of a single line, which reflects the presence of aromatic radical moieties with an unpaired electron spin delocalized in πp-type molecular orbitals (Uebersfeld *et al.,* 1954; Retcofsky *et al.,* 1968; Mrozowski, 1988b; Dickneider *et al.,* 1997). Several parameters can be deduced from the EPR spectra based on the amplitude, the linewidth, and the resonance field of the signal. Contrary to irradiation-induced defects in mineral hosts, radical defects in carbonaceous matter may not be due to natural irradiation and for this reason cannot be used for dating by monitoring the EPR intensity. Conversely, they are due to thermally activated reactions that occur during maturation of the organic matter. However, Skrzypczak-Bonduelle *et al.* (2008) proposed that the evolution of the EPR lineshape in insoluble organic matter could be used to estimate the age of primitive carbonaceous matter older than ~1 Gyr. More precisely, it was observed that the EPR lineshape evolves from Gaussian-Lorentzian for Phanerozoic cherts to purely Lorentzian for cherts older than ~1 Gyr and finally to stretched Lorentzian for cherts as old as 3.5 Gyr. This evolution was interpreted as a result of the variation of the spatial distribution of the electron spins in the carbonaceous matter. A lineshape factor (R_{10} factor) was defined to quantify the deviation of the signal from a Lorentzian shape. This parameter is equal to zero for a pure Lorentzian line, positive for an increasing Gaussian character, and negative for a stretched Lorentzian line (Skrzypczak-Bonduelle *et al.,* 2008). However, this proxy was initially based on a limited set of samples, and the potential contribution of metamorphism, as well as the precision of the method, had yet to be investigated.

In the present study, the R_{10} factor was calculated for numerous chert samples of various ages and metamorphic grades, all of which came from different locations. Carbonaceous matter resulting from thermally treated modern cyanobacterial samples was also studied in order to statistically test the robustness of the proxy. Since high temperature induces artificial aging, we also studied the EPR signals of three Silurian cherts that were the same age and had the same precursors but exhibited various metamorphic grades to clearly discriminate the effect of metamorphism from that of natural aging. Moreover, to test whether contamination by younger organic matter could be detected, a "contamination-like" mixture of fresh cyanobacteria and artificially aged cyanobacteria was designed and studied by EPR spectroscopy.

2. Material and Methods

2.1. Samples

Chert samples were selected that ranged widely in age, from the Silurian (~420 Myr) to the Archean (3.5 Gyr). These cherts are silicified sediments containing the carbonaceous remains of microorganisms (and macroorganisms in the most recent samples). The silica phase in the cherts is microcrystalline quartz. The samples originated from various localities: South Africa, Australia, North America, and Europe. The cherts had been exposed to different metamorphic events but always remained lower than or equal to the *greenschist* facies. This is a prerequisite for EPR studies given that, for higher metamorphic grades, organic matter inside the sample is further graphitized and thus no longer suitable. A description of the cherts studied is given in Table 1. We also reexamined the EPR spectra of cherts analyzed by Skrzypczak-Bonduelle *et al.* (2008), which are represented by letters in Table 1.

Microcoleus chthonoplastes cyanobacterial samples were collected in the lake "La Salada de Chiprana" (Ebro River basin, Northern Spain, 41°14′30″N, 0°10′50″W), the only permanent hypersaline ecosystem in Western Europe (Vidondo *et al.,* 1993). With a shallow-water environment, this lake represents a good analogue to an Archean environment and hosts extensive photosynthetic microbial mats. These mats have a multilayer structure and contain *M. chthonoplastes,* a

Table 1. Characteristics of the Cherts Studied (Identified by Numbers *1* to *11*)

N°	*Chert reference*	*Age (Gyr)*	*Location*	*Metamorphic grade*	*Described in*
1	PPRG456[a]	0.05	Clarno Formation, John Day Basin Tectonic Unit, Oregon, USA	n.m.	Schopf *et al.*, 1983
2	Zalesie Nowe[b]	0.42	Zalesie Nowe, Holy Cross Mountains, Bardo Syncline, Poland	*p.p.* to *p.a.*	Kremer and Kazmierczak, 2005
3	Zdanow[b]	0.42	Zdanow, Bardzkie Mountains, Sudetes Mountains, Poland	*p.p.* to *p.a.*	Kremer, 2006
4	Döbra[b]	0.42	Döbra, Franconian Forest, Bavaria, Germany	lower *g.s.*	Kremer *et al.*, 2012
5	3 of 06/30/84[c]	1.9	Gunflint Iron Formation, Port Arthur Homocline Tectonic Unit, Ontario, Canada	lower *g.s.*	Awramik and Barghoorn, 1977
6	3 of 10/25/92[c]	2.6	Jeerinah Formation, Fortescue Group, Hamersley Basin Tectonic Unit, Australia	*p.p.* to *p.a.*	/
7	99SA07[d]	3.3	Josefsdal Valley, Kromberg Formation, Onverwacht Group, Barberton Greenstone Belt, South Africa	*g.s.*	Westall *et al.*, 2006; Westall and Cavalazzi, 2011
8	99SA03[d]	3.3	Buck Reef, Kromberg Formation, Onverwacht Group, Barberton Greenstone Belt, South Africa	*g.s.*	Westall *et al.*, 2001
9	07SA22[d]	3.4	Middle Marker, Komati Formation, Barberton Greenstone Belt, South Africa	*g.s.*	/
10	07SA24[d]	3.4	Middle Marker, Komati Formation, Barberton Greenstone Belt, South Africa	*g.s.*	/
11	PPRG006[a]	3.5	Dresser Formation (former Towers Formation), Warrawoona Group, Pilbara Block, Australia	*p.p.* to lower *g.s.*	Schopf *et al.*, 1983
A	2 of 8/18/83[c]	1.6	Dahongyu Formation, Jixian section, Hebei, China	n.m.	/
B	7 of 8/18/83[c]	1.6	Dahongyu Formation, Jixian section, Hebei, China	n.m.	/
C	1 of 8/23/86[c]	1.9	Gunflint Iron Formation, Port Arthur Homocline Tectonic Unit, Ontario, Canada	lower *g.s.*	Awramik and Barghoorn, 1977
D	PPRG060[a]	2.0	Duck Creek Dolomite, Wyloo Group, Ashburton Trough Tectonic Unit, Australia	*p.a.*	Schopf *et al.*, 1983
E	6 of 10/25/92[c]	2.6	Jeerinah Formation, Fortescue Group, Hamersley Basin Tectonic Unit, Australia	*p.p.* to *p.a.*	/
F	PPRG002[a]	3.5	Dresser Formation (former Towers Formation), Warrawoona Group, Pilbara Block, Australia	*p.p.* to lower *g.s.*	Schopf *et al.*, 1983
G	2 of 16/09/65[c]	3.5	Upper Onverwacht Group, Barberton Greenstone Belt, South Africa	*g.s.*	/

Samples identified by letters A to G were previously studied in Skrzypczak-Bonduelle *et al.* (2008), but their spectra are reexamined in the present study. The cherts were collected by [a]J.W. Schopf, [b]B. Kremer, [c]S.M. Awramik, [d]F. Westall. The metamorphic facies are indicated as follows: n.m., non-metamorphosed; *p.p., prehnite-pumpellyite*; *p.a., pumpellyite-actinolite*; *g.s., greenschist*.

filamentous mat-building cyanobacterium that is common in marine and hypersaline environments, and therefore represent a good modern analogue of a Late Archean organism.

In October 2010, 20×10×10 cm blocks of microbial mats were sampled in La Salada de Chiprana and maintained in aquaria in the laboratory in aerated natural lake water, at ambient temperature and under Philips-HPI T Plus 400 W lamps. The microbial mats were dissected under magnifying glasses in order to separate *M. chthonoplastes* cyanobacteria from the rest of the mat. The separated cyanobacteria were rinsed two times with distilled water, frozen, and lyophilized.

2.2. Methods

Lyophilized bacteria (6 mg) was introduced in EPR tubes in quadruplicates for step heating treatment up to 620°C. Two tubes were then opened to recover the thermally treated bacteria, which were then mixed with 6 mg of intact lyophilized bacteria. The mixture was introduced in EPR tubes in duplicates. Intact chert rock (100 mg) was sampled and introduced in EPR tubes for analysis.

All EPR tubes were sealed under vacuum to avoid the presence of O_2, which can broaden the EPR line (Bates *et al.*, 1995). The accelerated aging was performed with a gradual step thermal treatment, from 70°C to 720°C. Each step consisted of a 50°C rise of temperature for 15 min, followed by the EPR measurement at room temperature (Skrzypczak-Bonduelle *et al.*, 2008).

Electron paramagnetic resonance analyses were performed on a Bruker ELEXSYS E500 spectrometer equipped with a high-sensitivity Bruker 4122SHQE/0111 microwave cavity. A microwave power ranging from 2 to 20 mW was used. All the experiments were conducted at ambient temperature and at X-band (9.5 GHz). Before each experiment,

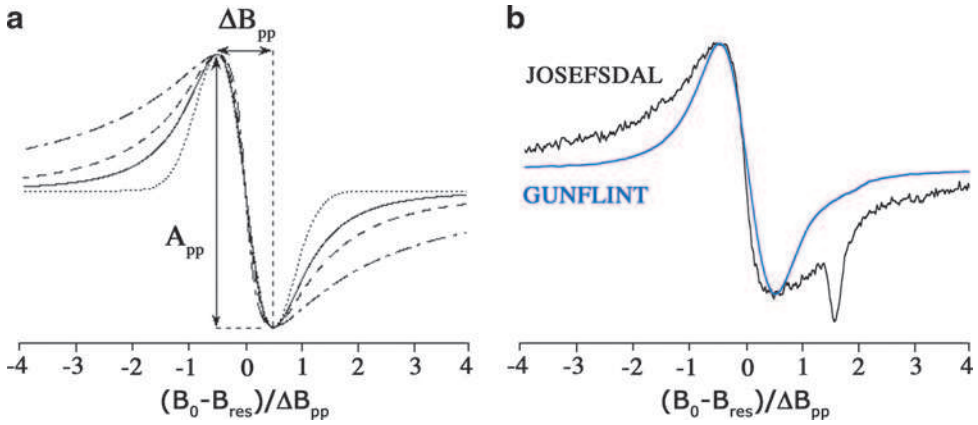

FIG. 1. (**a**) Theoretical EPR spectra corresponding to upper-limit cases of dipolar broadening. Dotted line: high spin concentration regime (Gaussian lineshape); Continuous line: diluted spin regime and 3-D distribution (Lorentzian lineshape); Dashed line: diluted regime, 2-D distribution (stretched Lorentzian); Mixed line: diluted regime, 1-D distribution (stretched Lorentzian). (**b**) EPR spectra at room temperature of organic radicals in the Gunflint chert and the Josefsdal chert. All EPR lines are normalized with respect to the linewidth. Color images available online at www.liebertonline.com/ast

the spectrometer was calibrated by using the diphenylpicrylhydrazyl (DPPH) standard with a known g factor ($g = 2.0037$).

The mathematical analysis of the EPR lineshape, which is the central part of this paper, is described in detail in the Appendix. All statistical tests, EPR parameters, and R_{10} factor calculations, together with their standard deviations, were performed in the literate programming style with Python to computation, with use of the open source Sage interface and the Numpy and Scipy libraries.

3. Results

3.1. EPR lineshape evolution in chert samples

The EPR line of organic radicals in Precambrian carbonaceous matter has the form of the first derivative of the absorption and can exhibit different lineshapes ranging from Gaussian to Lorentzian and stretched Lorentzian (Skrzypczak-Bonduelle *et al.*, 2008). These different lineshapes reflect the hydrogen content, the concentrated or diluted character of radicals in the carbonaceous matter, and the dimensionality of their spatial distribution. The different types of lineshapes are shown in Fig. 1a. When the electron spins are concentrated and/or when they interact with nuclear spins of hydrogen atoms present in the carbonaceous matter, the lineshape is intermediate between Lorentzian and Gaussian. When electron spins are less concentrated and randomly distributed in the volume of the carbonaceous matter (3-D distribution), the lineshape evolves to a pure Lorentzian. When the spins are distributed in a plane on aromatic layers (2-D distribution) or along a single direction on the edge of long aromatic layers (1-D distribution), the Lorentzian line is stretched, with wings falling off more slowly than a pure Lorentzian line (Fel'dman and Lacelle, 1996). The stretched character increases with the decreasing dimensionality of the spatial distribution.

Two examples of normalized EPR lines of carbonaceous radicals in Precambrian cherts are shown in Fig. 1b. The EPR spectrum of the Gunflint chert (blue spectrum) has the shape of a first derivative of a Lorentzian shape function, whereas the signature of the Josefsdal chert (black spectrum) exhibits a significant stretching in the wings. The narrow feature in the high field side of the carbon signal is due to oxygen vacancy centers (E' centers) in silica. As there are no analytical functions for such stretched Lorentzian signatures, we analyzed the EPR lines in a representation where a pure Lorentzian line is linear (Fig. 2). The new coordinates x and $f(x)$ are defined in the Appendix (Eq. A5). Any deviation from this line indicates a Gaussian contribution (positive deviation) or a stretching of the Lorentzian (negative deviation). By comparing the algebraic surface between the experimental data and the Lorentzian function plotted in the $\{x, f(x)\}$ representation, we defined a lineshape parameter (R_{10} factor), which measures the amount of Gaussian character ($R_{10} > 0$) and the amount of stretching of the Lorentzian line ($R_{10} < 0$), a pure Lorentzian line being characterized by $R_{10} = 0$ (Table 2). That is, the R_{10} factor will be greater than 0 for immature carbonaceous materials (young, no metamorphism), which have a high hydrogen/carbon (H/C) ratio in

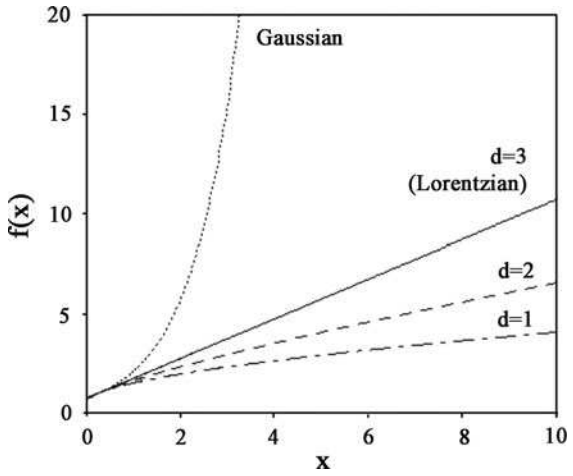

FIG. 2. Representation of the EPR spectra corresponding to the Gaussian, Lorentzian ($d = 3$) and lower-dimensional ($d = 1$ and 2) cases in the new (x, $f(x)$) coordinates system.

Table 2. EPR Lineshapes and the Lineshape R_{10} Factor for Different Limit Regimes of Dipolar Broadening

Regime	*Lineshape*	R_{10}
Concentrated spins	Gaussian-Lorentzian	>0
Diluted spins		
3-D distribution	Lorentzian	0
2-D distribution	Stretched Lorentzian	−1.78
1-D distribution	Stretched Lorentzian	−2.95

their radicals; equal to 0 for samples of intermediate maturity (older, metamorphosed), when the amount of organic radicals decreases and gets dilute and where H/C decreases; and less than 0 for samples of higher maturity (Archean) with very low H/C and for which aromatic layers start to orientate and thus induce a low-dimensional (2-D to 1-D) spatial distribution of the radicals.

Figure 3a shows the variation of the R_{10} factor with the age of the cherts. Numbers and letters represent chert samples analyzed in this study and by Skrzypczak-Bonduelle *et al.* (2008), respectively. Note that the R_{10} factor could only be calculated for samples having a symmetric EPR line at ambient temperature. It appears that the R_{10} factor decreases from $R_{10} \sim$ zero for Proterozoic samples of age ~1–1.5 Gyr to $R_{10} \sim -3$ for the oldest Archean samples (3.5 Gyr).

3.2. Step annealing treatments on immature chert and bacterial samples

The evolution of the R_{10} factor versus temperature during step annealing treatment of a young non-metamorphosed chert (Clarno chert, 45 Myr) and fresh cyanobacteria samples was investigated and reported in Fig. 3b (black symbols). The same evolution from a Lorentz-Gaussian shape to a stretched Lorentzian shape is observed by increasing step temperatures from 520°C to 720°C. R_{10} factor versus age (upper abscissa) of natural chert samples is also reported in Fig. 3b (red symbols) for comparison. The correlation between step annealing temperature (lower abscissa) and the age A in Gyr (upper abscissa) has been adjusted according to Skrzypczak-Bonduelle *et al.* (2008) by using Eq. 1:

$$T(^\circ\mathrm{C}) = 353 \ \log A - 2650 \qquad (1)$$

R_{10} factors were only calculated for each thermal treatment step of the bacteria at temperatures ≥500°C, because the intensity of the EPR signal was almost equal to zero for thermal treatment lower than 370°C. The R_{10} factor has no physical meaning for thermal treatment temperatures lower than 500°C; and it can be measured, but not used, for dating samples younger than 1 Gyr (Skrzypczak-Bonduelle *et al.*, 2008).

3.3. Step annealing treatment on Silurian chert samples

Three 0.42 Gyr old Silurian cherts (Zalesie Nowe, Zdanow, and Döbra, cherts n°2, 3, and 4) that originated from the same precursor but exhibit different metamorphic grades were studied in EPR (Fig. 4). Samples from Zalesie Nowe and Zdanow contain remarkably well-preserved microfossils, as well as fine crystalline chalcedony that has replaced

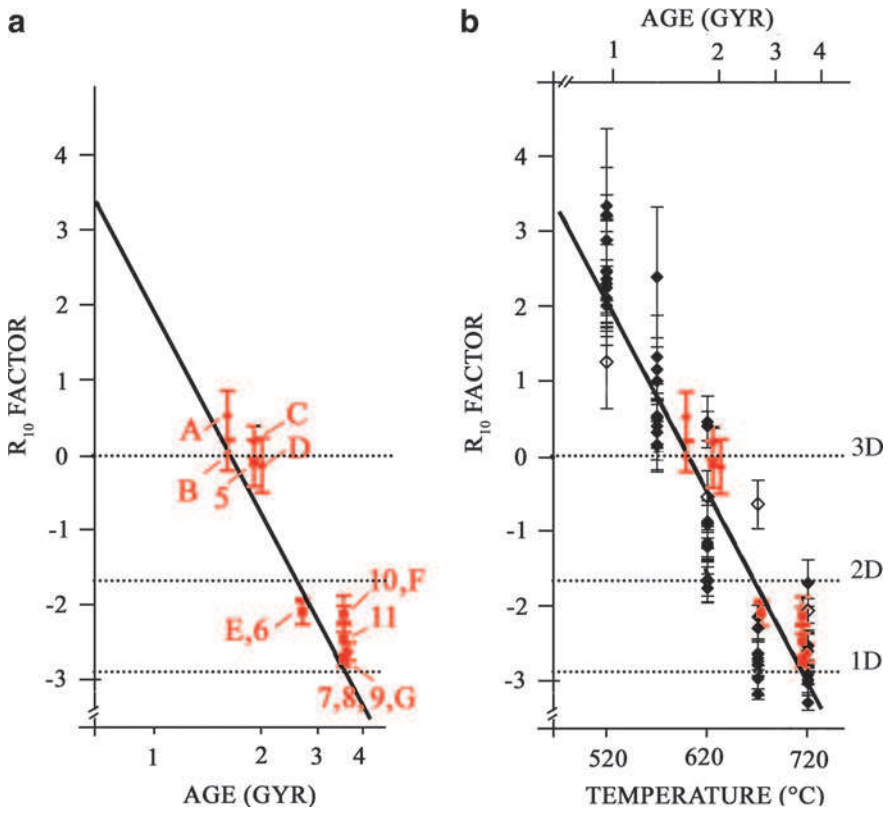

FIG. 3. (**a**) Evolution of the R_{10} factor with age of the chert samples. Numbers represent new samples examined in the present study, and letters represent samples studied by Skrzypczak-Bonduelle *et al.* (2008) and reexamined here. (**b**) Lower abscissa: evolution with temperature of the R_{10} factor for thermally treated cyanobacteria (full diamonds) and for the Clarno chert (open diamonds). Upper abscissa: evolution of the R_{10} factor with the age of the chert samples. Color images available online at www.liebertonline.com/ast

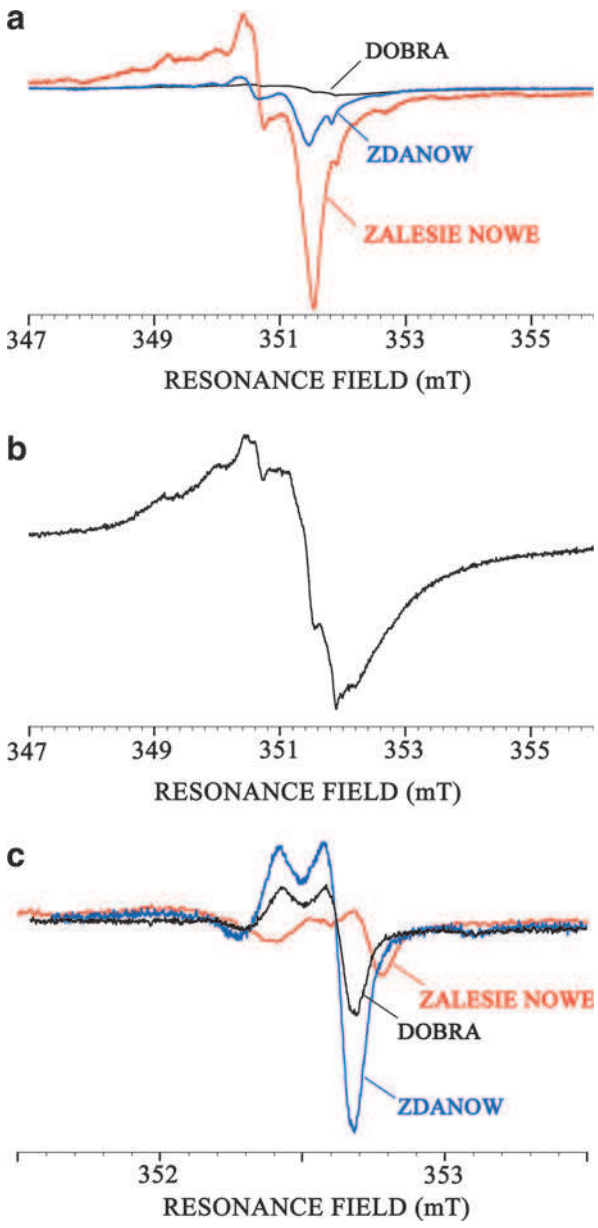

FIG. 4. X-band EPR spectra of the Silurian cherts recorded at room temperature (2 mW): (**a**) Zalesie Nowe, Zdanow, and (**b**) Döbra chert under in-phase detection and (**c**) 90° out-of-phase detection showing E′ centers in silica. Color images available online at www.liebertonline.com/ast

some primary opaline skeletons of radiolarians (Kremer and Kazmierczak, 2005). According to silica geothermometers, chalcedony is formed at relatively low temperature and is stable below 180°C (White and Corwin, 1961; Fournier and Potter, 1982). Therefore, the Zalesie Nowe and Zdanow samples may be classified in the *prehnite-pumpellyite* to *pumpellyite-actinolite* metamorphic facies, although geochemical thermal maturity parameters indicate that the Zdanow chert is thermally more altered than the Zalesie Nowe chert (Bauersachs *et al.*, 2009). The Döbra sample contains metamorphic minerals such as feldspars, quartz, and phyllosilicates (Kremer *et al.*, 2012), reflecting a higher metamorphic grade that ranges from *lower greenschist* to *greenschist* facies.

As a first observation, one can notice that the EPR signals are very complex. This was previously observed for cherts with ages ranging from Neogene to Paleozoic (Skrzypczak-Bonduelle *et al.*, 2008). The spectra of the less metamorphosed cherts (Zalesie Nowe and Zdanow) are nearly similar contrary to the most metamorphosed one (Döbra) (Figs. 4a, 4b). These signals are due to a variety of organic radicals and to defects in the mineral matrix. One of these signals can be recorded by 90° out-of-phase detection (Fig. 4c), indicating long relaxation times. This signature is typical of the well-known E′ center in SiO_2 (Jani *et al.*, 1983; Ikeya, 1993).

Cumulative thermal treatments were performed on the three aforementioned Silurian cherts (Fig. 5). For thermal treatment temperatures lower than 570°C, the EPR signal remained asymmetric, and no R_{10} factor could be calculated. For thermal treatment temperatures between 570°C and 620°C, a symmetric Lorentzian signal was obtained. However, disparities appear in R_{10} factor values (Fig. 5d), the less metamorphosed sample having a positive R_{10} factor, whereas the most metamorphosed one reveals a negative R_{10} factor. For thermal treatment temperatures higher than 670°C, the EPR signals evolved to a single stretched Lorentzian signal, which is independent of the initial metamorphic facies of the sample and similar to that of an Archean chert.

3.4. Step annealing treatments on a "contamination-like" mixture

A "contamination-like" mixture was obtained by mixing an equal amount of fresh *M. chthonoplastes* cyanobacteria with cyanobacteria that were thermally treated at 620°C, thus mimicking the presence of a recent contamination in a 2 Gyr old organic matter (see Fig. 3 and Eq. 1). The mixture was then treated again by the same step heating treatment as described above. The evolution of the R_{10} factor during thermal treatment of the EPR signal for noncontaminated *M. chthonoplastes* bacteria as well as for a "contamination-like" mixture is given in Fig. 6.

The R_{10} factor for pure *M. chthonoplastes* cyanobacteria (red circles) has a classic evolution with thermal treatment, from a positive R_{10} factor value to a negative one, in agreement with Eq. 2. On the contrary, when recording the EPR signal of the "contamination-like" mixture at ambient temperature, the R_{10} factor already had a negative value ~ -2, similar to the value of a very primitive organic matter (Fig. 3). When performing thermal treatment on the "contamination-like" sample, the R_{10} factor increases for thermal treatment temperatures up to 520°C and then decreases (black squares on Fig. 6).

3.5. Step annealing treatments on Archean cherts

The evolution of the R_{10} factor during thermal treatment of three Archean (3.3–3.5 Gyr) chert samples—the Josefsdal, the Middle Marker, and the Dresser cherts—is reported in Fig. 7a. It was compared to the evolution of the R_{10} factor during thermal treatment of the Silurian cherts (420 Myr) and the Clarno chert (45 Myr), as well as the chert samples from Rhynie (396 Myr) and Gunflint (1.9 Gyr) (Skrzypczak-Bonduelle *et al.*, 2008). The R_{10} factor of Archean cherts remained ≤ -2 until the equivalent age of the sample was attained.

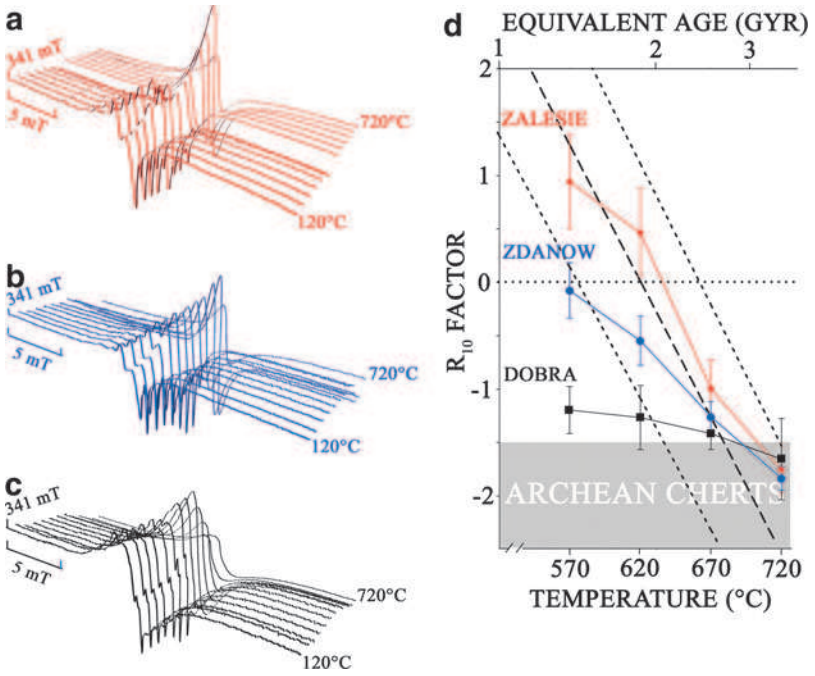

FIG. 5. Evolution of the EPR signals during step thermal treatment of (**a**) the Zalesie Nowe chert, (**b**) the Zdanow chert, (**c**) the Döbra chert, and (**d**) the calculated R_{10} factors. The correlation of R_{10} factor with age is given in dashed line with its error margin. Equivalent age is given in the upper abscissa. Color images available online at www.liebertonline.com/ast

Three types of sample were distinguished, as summarized in Fig. 7b:

(i) Immature samples, that is, young and low-metamorphic grade samples, such as carbonaceous matter from recent microorganisms or the Clarno (Eocene) and the Rhynie (Devonian) cherts.
(ii) Samples of intermediate maturity, that is, Proterozoic and Phanerozoic cherts with a metamorphism lower than or equal to the *greenschist* facies, such as the Silurian cherts and the Gunflint chert.
(iii) Archean samples, that is, older than 2.5 Gyr, such as the Josefsdal, the Middle Marker, and the Dresser cherts.

The evolution of immature samples during thermal treatment followed the R_{10} factor/age correlation during cumulative thermal treatments (red area on Fig. 7b), whereas Archean samples remained stable, with R_{10} values ranging from -1.5 to $-l3$ (gray area in Fig.7b). The evolution of intermediate samples falls between those two extreme zones (blue zone in Fig. 7b).

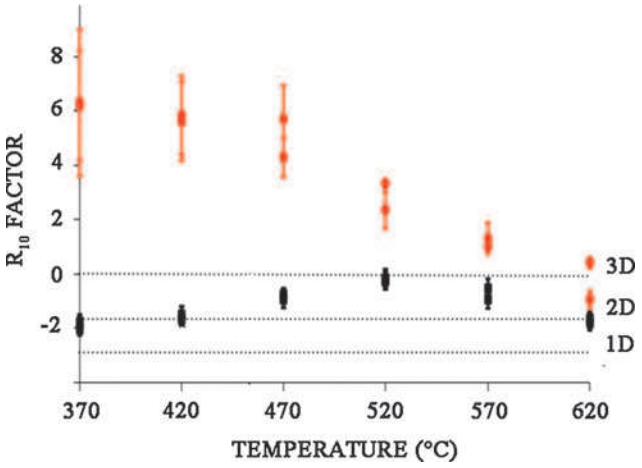

FIG. 6. Evolution of the R_{10} factor during thermal treatment of noncontaminated *M. chthonoplastes* bacteria (circles) and the "contamination-like" mixture (squares). Color images available online at www.liebertonline.com/ast

4. Discussion

4.1. Generalizing the age/R_{10} factor correlation

Previous experiments (Sections 3.1–3.3) showed a correlation between the age of the sample and the lineshape R_{10} factor for samples reaching an age or an equivalent age older than 1 Gyr. The R_{10} factor decreases from $R_{10} \sim$ zero for Proterozoic samples of age $\sim$1–1.5 Gyr to $R_{10} \sim -3$ for the oldest Archean samples (3.5 Gyr). This reflects the evolution of the lineshape from a 3-D spatial distribution of spins for 1.5 Gyr old cherts to a 2-D to 1-D spatial distribution of spins for 3.5 Gyr old cherts.

The parameters of the equation of the aforementioned correlation were computed with the help of a Monte Carlo simulation based on the standard deviation of each point. It must be noted that the correlation was established empirically. The robustness of the equation was checked by testing for the effect of outliers on the parameters (see Appendix). The following equation was obtained:

$$R_{10} = \alpha \cdot \log A + \beta \qquad (2)$$

with A in Gyr, $\alpha = -9.0 \pm 0.3$, and $\beta = 83.0 \pm 2.9$. The equation coefficients are different from those obtained by Skrzypczak-Bonduelle *et al.* (2008), where

$$\alpha = -5.3 \pm 0.4 \text{ and } \beta = 48.9 \pm 0.9$$

This is not due to implementation of the R_{10} factor calculation, given that, when fitted with the present method for checking, spectra obtained by Skrzypczak-Bonduelle *et al.* (2008) led to similar R_{10} factor values. There are two main reasons for this discrepancy: (i) new data were incorporated to the distribution

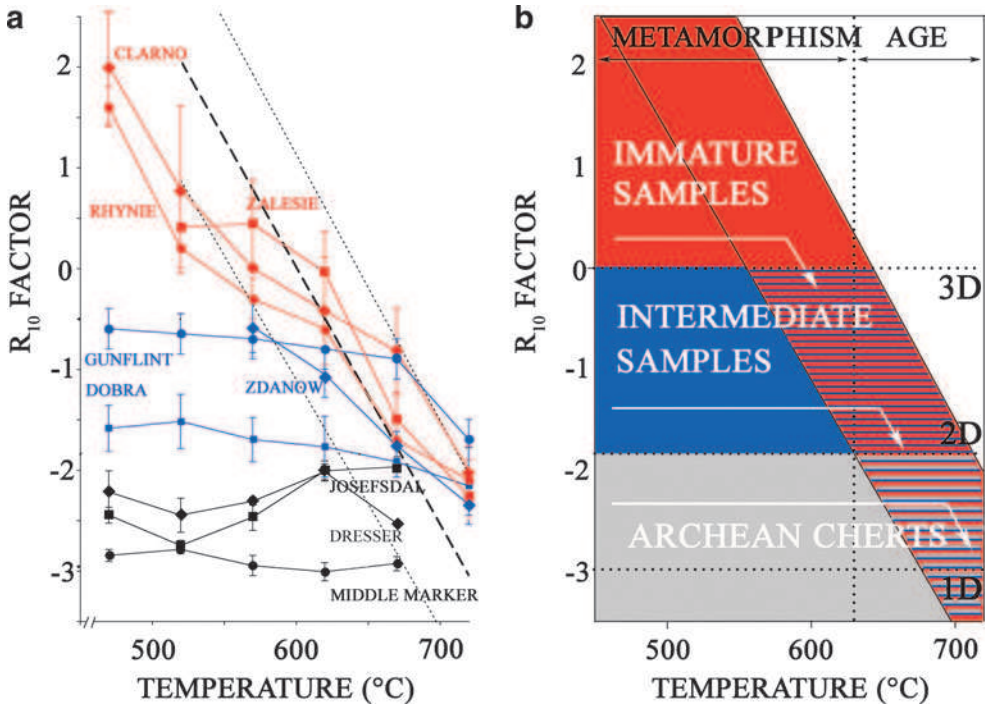

FIG. 7. (**a**) Evolution of the R_{10} factor during thermal treatment of chert samples from Clarno (diamonds), Zalesie Nowe (squares), Rhynie (circles), Zdanow (diamonds), Gunflint (circles), Döbra (squares), Josefsdal (squares), the Middle Marker (circles), and the Dresser (diamonds). (**b**) Corresponding scheme of the evolution of R_{10} upon heating treatments of immature samples, samples of intermediate maturity, and Archean samples. Color images available online at www.liebertonline.com/ast

and (ii) the equation obtained by Skrzypczak-Bonduelle *et al.* (2008) took into account cherts of ages lower than 1 Gyr, whereas the newly proposed equation is established for chert samples older than 1 Gyr only, where the use of R_{10} factor is relevant. It must also be noted that the accuracy of the age determination is not better than that of Skrzypczak-Bonduelle, but the correlation is now considered more robust.

This study confirms the occurrence of a correlation between the age of the chert sample and the lineshape R_{10} factor of the carbonaceous matter for cherts older than 1 Gyr. Equation 2 may be inverted, which would allow dating of the carbonaceous matter in a chert from the calculation of its R_{10} factor. However, it may be argued that this evolution could only reflect the influence of thermally activated processes that occurred during the thermal history of the samples. Therefore, the effect of thermal metamorphism had to be investigated.

4.2. Impact of thermal metamorphism

By examining data of Fig. 3b, where a short thermal treatment of fresh samples (bacteria) or young cherts has the same effect as evolution over long geological times, it can be anticipated that metamorphism may affect the EPR signal of the carbonaceous matter embedded in a chert. Namely, even under the *greenschist* facies, metamorphism is likely to modify the composition, texture, and structure of the organic matter, affecting its EPR signal.

However, the complexity of the spectra of the Silurian cherts described in Section 3.3, even for the most metamorphosed sample, shows that they are very different from spectra of Precambrian cherts. This is consistent with their young age, as previously shown for cherts of the Clarno Formation (45 Myr) and the Rhynie Formation (396 Myr) (Skrzypczak-Bonduelle *et al.*, 2008). However, the latter cherts were not metamorphosed. These results demonstrate that, although metamorphism (lower than or equal to *greenschist*) has an impact on the EPR spectrum, even the most metamorphosed Phanerozoic chert did not show an EPR spectrum comparable to that of Archean cherts. In other words, a single line with a stretched Lorentzian shape, and therefore a negative R_{10} factor value, cannot be reached only with a high metamorphic facies of a young sample.

Disparities appear in R_{10} factor values (Fig. 5d), the less metamorphosed sample having a positive R_{10} factor, whereas the most metamorphosed one reveals a negative R_{10} factor. This can be explained by the fact that the most metamorphosed sample had already lost heteroelements and hydrogen during its metamorphic history. This is not the case for the less metamorphosed sample, which undergoes heteroelement and hydrogen loss (and therefore 3-D creation of radicals) only during thermal treatment, driving the R_{10} factor to a positive value until radical recombination occurs. For thermal treatment temperatures higher than 670°C, the EPR signals evolved to a single stretched Lorentzian signal independently of the initial metamorphic facies of the sample. Namely, when considering the evolution of R_{10} factor values during thermal treatment higher or equal to 670°C (Fig. 5d), the effect of previous thermal events becomes negligible, and all the data correlate well with the previously established equation (Eq. 2). This shows that, for thermal treatment temperatures lower than 670°C, the EPR spectrum reflects both the age and the metamorphic grade of the sample,

whereas for thermal treatment temperatures higher than or equal to 670°C, only the age of the sample is important.

This phenomenon may be understood when considering carbonization kinetics that controls the maturation of the kerogen, which is estimated to be a first-order reaction (Singer and Lewis, 1978). That is, the amount of radicals N_{rad} created at time t is proportional to

$$N_{rad} \propto \exp\ (-kt) \tag{3}$$

where k is the kinetic constant given by the Arrhenius law:

$$k = A\ \exp\left(-\frac{E_a}{RT}\right) \tag{4}$$

where A is the collision constant (s^{-1}), E_a the activation energy ($J \cdot mol^{-1}$), R the gas constant ($J \cdot mol^{-1} \cdot K^{-1}$), and T the temperature (K). The intensity of an EPR spectrum, which is related to the number of spins $N_{rad}(t,T)$ produced during carbonization of the organic matter, thus depends on both time t and temperature T. The kinetic equation indicates that the same amount of radicals can be created during carbonization by using two different time-temperature couples (t_1, T_1) and (t_2, T_2) (Mrozowski, 1988a, 1988b):

$$t_1 \cdot \exp\left(-\frac{E_a}{RT_1}\right) = t_2\ \cdot \exp\left(-\frac{E_a}{RT_2}\right) \tag{5}$$

This implies that 1 Gyr at 300°C creates as many spins as 5 min at 670°C (Mrozowski, 1988a,b). Within the scope of this study, only cherts with a metamorphism lower or equal to *greenschist* have been studied. Therefore, the number of radicals in such Archean cherts (older than 2.5 Gyr) is driven by time rather than metamorphism.

It may be concluded that low-metamorphic grade Archean organic matter can be dated by using the shape of its EPR spectrum. However, it must be determined whether contamination during or after the Proterozoic, when more modern forms of life existed, may be detected.

4.3. Methodology for contamination detection

As shown in Fig. 6 and described in Section 3.4, without cumulative thermal treatment, contamination could not be detected because of its low (or lack of) contribution to the EPR signal, as compared to the most mature fraction. This means that genuine Archean organic matter cannot be distinguished from organic matter contaminated by a younger one on the sole basis of the R_{10} factor value.

However, when performing thermal treatment on the "contamination-like" sample, the R_{10} factor increases for thermal treatment temperatures up to 520°C and then decreases (black squares on Fig. 6). As discussed earlier, such an evolution is consistent with the 3-D creation of radicals and chemical transformation (loss of heteroelements and then hydrogen) within the organic matter of the contaminating cyanobacteria, which were not preheated (*i.e.*, corresponding to the most recent fraction of the mixture), and subsequent evolution toward a lower dimension (2-D and 1-D) of their distribution (decrease in R_{10}). The EPR signal of the preheated cyanobacterial component of the mixture is not sensitive to thermal treatment temperatures lower than 620°C, given that chemical transformations have already taken place and radicals were already in existence. Thus, the evolution of the R_{10} factor for thermal treatment lower than the temperature equivalent to the age of the sample (as calculated by using the time versus thermal treatment temperature equivalency given in Eq. 1) documents the presence of a less mature fraction, that is, a contamination. If no contamination occurred, the R_{10} value should be steady through the thermal treatment process.

This study highlights that a single EPR measurement on mature organic material is not sufficient to detect contamination. This leads us to propose the following methodology of contamination detection:

(i) Cumulative thermal treatment of material in EPR tubes sealed under vacuum (as described in the Material and Methods section)
(ii) Subsequent EPR analysis and calculation of the R_{10} factor.
(iii) If no contamination is detected, the age of the organic matter can be determined. If a contamination is detected, only the age of the oldest fraction of the organic matter can be determined.

When applying this contamination detection methodology to three Archean cherts (Josefsdal, Middle Marker, Dresser) (Fig. 7), the R_{10} factor of the cherts remained ≤ -2 until the equivalent age of the sample was attained. However, a slight increase in R_{10} in the Josefsdal and Dresser samples was detected. This could be the signature of a weak contamination. To elucidate this phenomenon, the study of more "contamination-like" mixtures with decreasing contamination rates is necessary.

5. Conclusions

This study demonstrates the strength of EPR as an emerging tool for dating and kerogen syngeneity assessment in cherts of Archean age. More specifically, the evolution of the lineshape, which progressively deviates from Lorentzian ($\sim$2 Gyr) toward stretched Lorentzian ($\sim$3.5 Gyr), is a good marker of the age of Archean organic matter. The lineshape factor (R_{10} factor) proposed by Skrzypczak-Bonduelle *et al.* (2008) to measure this evolution was generalized, and the robustness of its correlation with age of the sample was statistically tested. However, the accuracy of age determination was not better than that of this previous work. It was also shown that the R_{10} factor of Archean cherts is not driven by metamorphism for metamorphic grades lower than or equal to the *greenschist* facies. Moreover, it is possible to detect an organic contamination in Archean cherts by monitoring the R_{10} factor upon cumulative thermal treatments. Such experiments were run on samples of various age and metamorphism, demonstrating that metamorphism controls the EPR lineshape for samples younger than 2 Gyr and that only the age controls the lineshape for samples older than 2 Gyr. Such a dating method on low-metamorphic grade Archean samples could be used in further exobiology studies, for instance, on returned rocks from Mars.

Appendix A

Definition of an EPR lineshape parameter

The shape of the magnetic resonance absorption line of a system of interacting and randomly distributed spins

depends on the nature of the interactions (dipole-dipole or exchange), the spin concentration, and the dimensionality (1-D to 3-D) of the spatial distribution of the spins (Van Vleck, 1948; Kittel and Abrahams, 1953; Drabold and Fedders, 1988; Bencini and Gatteschi, 1990; Fel'dman and Lacelle, 1996). The present study is restricted to the case of a dipole-dipole–type interaction between electron spins, excluding exchange interaction occurring in very concentrated electron spin systems. Several limiting cases can be distinguished, depending on the spin concentration and on the dimensionality of the distribution.

In the high-concentration regime (generally considered when the fractional site occupation f by a paramagnetic center exceeds 0.1), the lineshape is approximately Gaussian (Kittel and Abrahams, 1953). This regime also occurs when the EPR line is broadened by unresolved hyperfine interaction with hydrogen nuclei. Given that experimental EPR spectra correspond to absorption derivatives, the Gaussian line is described by

$$F_G(B_0 - B_{res}) = -A_{pp} \cdot \frac{B_0 - B_{res}}{\Delta B_{pp}} \cdot \exp\left[-2\left(\frac{B_0 - B_{res}}{\Delta B_{pp}}\right)^2 + \frac{1}{2}\right] \quad \text{(A1)}$$

where B_0 is the applied magnetic field, B_{res} the field at the center of the line (maximum of absorption), A_{pp} the peak-to-peak amplitude, and ΔB_{pp} the peak-to-peak linewidth (Fig. 1a).

In the low-concentration regime (generally considered when $f < 0.01$) and with no hyperfine broadening, the lineshape depends on the dimensionality of the spatial distribution of the paramagnetic centers (Fel'dman and Lacelle, 1996). When the distribution is random, the resonance line may be calculated from the relaxation function:

$$G_d(t) = B \cdot \exp\left(-a \cdot t^{d/3}\right) \quad \text{(A2)}$$

This function describes the decay with time t of the spin magnetization, perpendicular to the magnetic field, after an infinitely short microwave pulse. a is a constant that depends linearly on the spin concentration, and parameter d represents the dimensionality of the spin distribution: $d = 1$ for a linear distribution, $d = 2$ for a distribution in a plane, and $d = 3$ for a distribution in a volume. The EPR absorption is the Fourier transform of the relaxation function; thus the EPR spectrum is the field derivative of this Fourier transform given by

$$F_d(B_0 - B_{res}) = \mathrm{Re}\left\{\int_0^{+\infty} G_0(t)\left(-i\frac{g\beta}{\hbar}t\right)\exp\left[-i\frac{g\beta}{\hbar}(B_0 - B_{res})t\right]dt\right\} \quad \text{(A3)}$$

where Re stands for the real part. In the case of a three-dimensional distribution ($d = 3$), the EPR lineshape function can be analytically calculated and corresponds to the field derivative of a Lorentzian function:

$$F_3(B_0 - B_{res}) = -\frac{16}{9}A_{pp}\frac{(B_0 - B_{res})/\Delta B_{pp}}{\left[1 + \frac{4}{3}\left((B_0 - B_{res})/\Delta B_{pp}\right)^2\right]^2} \quad \text{(A4)}$$

For lower-dimensional cases ($d < 3$), the Fourier transform can only be calculated numerically. Figure 1a shows the theoretical EPR spectra corresponding to the Gaussian, Lorentzian ($d = 3$), and lower-dimensional ($d = 1$ and 2) cases. The wings of a Gaussian line fall off faster than those of a Lorentzian line, while the wings of an EPR spectrum corresponding to a lower-dimensional distribution fall off more slowly, giving rise to a stretched Lorentzian lineshape. For a graphical comparison of the different lineshapes, it is more convenient to use a system of coordinates (x, y) such that

$$x = \left(\frac{B_0 - B_{res}}{\Delta B_{pp}}\right)^2$$

and

$$y = f(x) = \sqrt{\frac{A_{pp}}{F(B_0 - B_{res})} \cdot \frac{B_0 - B_{res}}{\Delta B_{pp}}} \quad \text{(A5)}$$

where $F = F_d$ or F_G. In this representation (Fig. 2), the Lorentzian case is represented by a straight line of equation:

$$f_L(x) = x + \frac{3}{4} \quad \text{(A6)}$$

and the Gaussian shape by an increasing exponential:

$$f_G(x) = \exp\left(x - \frac{1}{4}\right) \quad \text{(A7)}$$

with $f_G(x) \geq f_L(x), \forall x$

For diluted spin systems with low dimensional distribution, the representative curve $f_d(x)$ lies below the line (Eq. A6) corresponding to a Lorentzian shape. To quantitatively characterize the lineshape for systems intermediate between the above four ideal cases [Gaussian, Lorentzian ($d = 3$), one-dimensional ($d = 1$), and two-dimensional ($d = 2$)], we define a lineshape parameter by measuring the deviation from a Lorentzian line and given by (Skrzypczak-Bonduelle *et al.*, 2008):

$$R_{10} = \frac{1}{10}\int_{x=0}^{x=10} [f(x) - f_L(x)]dx \quad \text{(A8)}$$

This parameter corresponds to the algebraic surface between the curve $f(x)$ that represents an experimental EPR spectrum and the curve $f_L(x)$ that represents a Lorentzian line. R_{10} is negative for a low-dimensional distribution ($d < 3$) and positive for an EPR line intermediate between Lorentzian and Gaussian lines (Table 2). The integration in Eq. A8 must be restricted to a finite range of x values, for the integral may not converge when $x \to \infty$. In practice, the range is limited to $x \leq 10$, since in most cases encountered the signal-to-noise ratio of the EPR spectra is poor for $x \geq 10$, inducing strong fluctuations in $f(x)$ and consequently in the lineshape parameter.

Implementation of a standardized evaluation of R_{10}

The large-scale background signal of EPR spectra was first subtracted with a second-degree polynomial fitted on the smooth parts of the spectrum. The latter is defined as the part of the spectrum that is close to the baseline, which corresponds in practice to the first and last 200 data points in a typical spectrum. The observed fluctuations in those parts are only due to noise. In the following, *the spectrum* will be understood as the baseline corrected raw spectrum.

To uncover the underlying Lorentzian curve, which is compared to the original spectrum for the R_{10} computation, we need to find the three parameters that determine the latter, that is, the peak-to-peak amplitude A_{pp}, the linewidth ΔB_{pp}, and the resonance field B_{res}. We define the peaks (positive and negative) as the extrema of the spectrum, A_{pp} as the difference between the ordinate of the extrema, and ΔB_{pp} as the difference between their abscissas. The resonance field is defined as the value at which the EPR lineshape crosses the zero axis.

We need to compute the error bars on the three parameters in order to propagate them in the global R_{10} error calculation. For that we use a bootstrap method, in which the noise is considered to originate from a Poisson process (counting), and the standard deviation on each data point is taken to be the square root of its ordinate value. With this method, a large number of cloned data sets is generated, for which A_{pp}, ΔB_{pp}, and B_{res} are measured, thus giving the distribution for each parameter. All three distributions are normal, as expected. We thus take the final three parameter values as the average of the three distributions, respectively, and the error as the standard deviation.

R_{10} calculation, as described above in Eq. A8, is a function of A_{pp}, ΔB_{pp}, and B_{res}. A Monte Carlo simulation was implemented by using previously obtained standard deviations on those values in order to access a distribution of R_{10} factor values. Again, the distribution turned out to be normal, as expected. The R_{10} value was thus taken as the average of the final distribution and the error as the standard deviation.

The R_{10} measurement procedure is difficult for two reasons: (i) the inherent noise of the measurements and (ii) the short-scale background signals, such as E′ radicals in silica, which often make the spectrum slightly asymmetric. To solve (i), the inherent noise is taken to be the noise propagated from the errors on A_{pp}, ΔB_{pp}, and B_{res}. To solve (ii), the R_{10} measurement is performed on both sides of the spectrum (side being defined relative to the resonance field B_{res}) and the two values averaged.

Computing the equation between the R_{10} factor and the age of the carbonaceous matter

A list of three values was generated for each sample: the sample age (as calculated by geochemical studies in which U-Pb isotopic data were used), the R_{10} factor, and its standard deviation. The error bar on sample age was considered to be negligible, usually 1% of the value.

Having observed a linear dependence between the R_{10} factor and the logarithm of the age (Fig. 3 in the text), we empirically modeled the R_{10} dependence on age as

$$R_{10} = \alpha \cdot \log A + \beta \tag{A9}$$

We then fitted the value of α and β, and the distribution on those parameters was obtained from a Monte Carlo simulation based on the previously computed R_{10} factor standard deviation. Once again, each distribution turned out to be normal, and the α and β values and standard deviations were thus taken as the average and standard deviation of the respective distributions.

The robustness of the equation was assessed by testing the sensitivity of the results to outliers; after removing each data point one at a time, the equation was computed on all other data points. We found that the resulting values of α and β lay within the boundaries of their previously computed distributions, which shows that no data point radically modifies the equation coefficients and thus proves the robustness of the method.

To find the age of a sample given the R_{10} factor, we need to inverse Eq. A9. Again, to assess the quality of the values for the age thus found, we need to compute the distribution of the age given the errors on α, β, and R_{10}. A Monte Carlo simulation is thus performed by using the standard deviation on R_{10} and the list of [α, β] values previously obtained. We stress the fact that the α and β values are correlated variables that must be considered as a couple and not independently.

Acknowledgments

This work was supported by the Exobiology group of the CNES (Centre National d'Etudes Spatiales), the PNP (Programme National de Planétologie) program of the CNRS (Centre National de la Recherche Scientifique), and the NCN grant NN307468938 (B.K.). The authors wish to thank Frederic Mentink-Vigier for his constructive discussions on EPR experiments and the TGE-RENARD facility.

Author Disclosure Statement

No competing financial interests exist.

Abbreviations

EPR, electron paramagnetic resonance; NanoSIMS, nanoscale secondary ion mass spectrometry.

References

Awramik, S.M. and Barghoorn, E.S. (1977) The Gunflint microbiota. *Precambrian Res* 5:121–142.

Bates, S., Yetkin, Z., Jesmanowicz, A., Hyde, J.S., Bandettini, P.A., Estkowski, L., and Haughton, V.M. (1995) Artifacts in functional magnetic resonance imaging from gaseous oxygen. *J Magn Reson Imaging* 5:443–445.

Bauersachs, T., Kremer, B., Schouten, S., and Sinninghe Damsté, J.S. (2009) Biomarker and δ^{15}N study of thermally altered Silurian cyanobacterial mats. *Org Geochem* 40:149–157.

Bencini, A. and Gatteschi, D. (1990) Exchange narrowing in lower dimensional systems. In *EPR of Exchange Coupled Systems*, Springer-Verlag, Berlin, pp 155–157.

Binet, L., Gourier, D., Derenne, S., and Robert, F. (2002) Heterogeneous distribution of paramagnetic radicals in insoluble organic matter from the Orgueil and Murchison meteorites. *Geochim Cosmochim Acta* 66:4177–4186.

Binet, L., Gourier, D., Derenne, S., Robert, F., and Ciofini, I. (2004) Occurrence of abundant diradicaloid moieties in the insoluble organic matter from the Orgueil and Murchison meteorites: a fingerprint of its extraterrestrial origin? *Geochim Cosmochim Acta* 68:881–891.

Buick, R. (1990) Microfossil recognition in Archean rocks: an appraisal of spheroids and filaments from a 3500 Myr old chert-barite unit at North Pole, Western Australia. *Palaios* 5:441–459.

Campbell, S.E. (1982) Precambrian endoliths discovered. *Nature* 299:429–431.

Delpoux, O., Gourier, D., Vezin, H., Binet, L., Derenne, S., and Robert, F. (2011) Biradical character of the D-rich carriers in the insoluble organic matter of carbonaceous chondrites: a relic of the protoplanetary chemistry. *Geochim Cosmochim Acta* 75:326–336.

Dickneider, T.A., Scull, S., Whelan, J.K., and Blough, N.V. (1997) EPR study of kerogens from Middle Valley, Northern Juan de Fuca Ridge. *Org Geochem* 26:341–352.

Drabold, D.A. and Fedders, P.A. (1988) Dipolar broadening in magnetically diluted lattices. *Phys Rev B Condens Matter Mater Phys* 37:3440–3447.

Faure, G. (1986) *Principles of Isotope Geochemistry*, edited by G. Faure, Wiley & Sons, New York.

Fel'dman, E.B. and Lacelle, S. (1996) Configurational averaging of dipolar interactions in magnetically diluted spin networks. *J Chem Phys* 104:2000–2010.

Fournier, R.O. and Potter, R.W. (1982) A revised and expanded silica (quartz) geothermometer. *Geothermal Resources Council Bulletin* 11–10:3–12.

Gourier, D., Robert, F., Delpoux, O., Binet, L., Vezin, H., Moissette, A., and Derenne, S. (2008) Extreme deuterium enrichment of organic radicals in the Orgueil meteorite: revisiting the interstellar interpretation? *Geochim Cosmochim Acta* 72:1914–1923.

Hoering, T.C. (1966) Criteria for suitable rocks in Precambrian organic geochemistry. *Year B Carnegie Inst Wash* 65:365–372.

Hoering, T.C. (1967) The organic geochemistry of Precambrian rocks. In *Researches in Geochemistry*, Vol. 2, edited by P.H. Abelson, John Wiley, New York, pp 87–111.

Ikeya, M. (1993) SiO_2: rocks, faults and sediments. In *New Applications of Electron Spin Resonance: Dating, Dosimetry and Microscopy*, edited by M. Ikeya, World Scientific Publishing, Singapore, pp 271–314.

Jani, M.G., Bossoli, R.B., and Halliburton, L.E. (1983) Further characterization of the E'_1 center in crystalline SiO_2. *Phys Rev B Condens Matter Mater Phys* 27:2285–2293.

Kittel, C. and Abrahams, E. (1953) Dipolar broadening of magnetic resonance lines in magnetically diluted crystals. *Phys Rev* 90:238–239.

Knoll, A.H., Golubic, S., Green, J., and Swett, K. (1986) Organically preserved microbial endoliths from the Late Proterozoic of East Greenland. *Nature* 321:856–857.

Kremer, B. (2006) Mat-forming coccoid cyanobacteria from early Silurian marine deposits of Sudetes, Poland. *Acta Palaeontologica Polonica* 51:143–154.

Kremer, B. and Kazmierczak, J. (2005) Cyanobacterial mats from Silurian black radiolarian cherts: phototrophic life at the edge of darkness? *Journal of Sedimentary Research* 75:897–906.

Kremer, B., Bauer, M., Stark, R.W., Gast, N., Altermann, W., Gursky, H.J., Heckl, W.M., and Kazmierczak, J. (2012) Laser-Raman and atomic force microscopy assessment of the chlorococcalean affinity of problematic microfossils. *J Raman Spectrosc* 43:32–39.

Mrozowski, S. (1988a) ESR studies of carbonization and coalification processes part I: carbonaceous compounds. *Carbon* 26:521–529.

Mrozowski, S. (1988b) ESR studies of carbonization and coalification processes part II: biological materials. *Carbon* 26:531–541.

Oehler, D.Z., Robert, F., Walter, M.R., Sugitani, K., Allwood, A., Meibom, A., Mostefaoui, S., Selo, M., Thomen, A., and Gibson, E.K. (2009) NanoSIMS: insights to biogenicity and syngeneity of Archean carbonaceous structures. *Precambrian Res* 173:70–78.

Porat, N. and Schwarcz, H.O. (1991) Use of signal subtraction methods in ESR dating of burned flint. *Nucl Tracks Radiat Meas* 18:203–212.

Retcofsky, H.L., Stark, J.M., and Friedel, R.A. (1968) Electron spin resonance in American coals. *Anal Chem* 40:1699–1704.

Robert, F., Oehler, D., Chaussidon, M., Mostefaoui, S., Meibom, A., and Gibson, E. (2008) Obtaining valid data from NanoSIMS and SIMS for assessment of early Archean biogenicity. In *XV International Conference on the Origin of Life (ISSOL)*, Florence, Italy.

Robins, G.V., Seeley, N.J., McNeil, D.A.C., and Symons, M.C.R. (1978) Identification of ancient heat treatment in flint artefacts by ESR spectroscopy. *Nature* 276:703–704.

Roedder, E. (1981) Are the 3800-Myr-old Isua objects microfossils, limonite-stained fluid inclusions, or neither? *Nature* 293:159–162.

Schopf, J.W., Hayes, J.M., and Walter, M.R. (1983) Evolution of Earth's earliest ecosystems: recent progress and unsolved problems. In *Earth's Earliest Biosphere*, edited by J.W. Schopf, Princeton University Press, Princeton, NJ, pp 361–384.

Singer, L.S. and Lewis, I.C. (1978) ESR study of the kinetics of carbonization. *Carbon* 16:417–423.

Skinner, A.R. (2000) ESR dating: is it still an "experimental" technique? *Appl Radiat Isot* 52:1311–1316.

Skrzypczak-Bonduelle, A., Binet, L., Delpoux, O., Vezin, H., Derenne, S., Robert, F., and Gourier, D. (2008) EPR of radicals in primitive organic matter: a tool for the search of biosignatures of the most ancient traces of life. *Appl Magn Reson* 33:371–397.

Uebersfeld, J. and Erb, E. (1956) A new effect of oxygen on the paramagnetic resonance of charcoal. *Comptes Rendus de l'Académie des Sciences (Paris)* 243:363–364.

Uebersfeld, J., Etienne, A., and Combrisson, J. (1954) Paramagnetic resonance, a new property of coal-like materials. *Nature* 174:614.

Van Vleck, J.H. (1948) The dipolar broadening of magnetic resonance lines in crystals. *Phys Rev* 74:1168–1183.

Vidondo, B., Martinez, B., Montes, C., and Guerrero, M.C. (1993) Physico-chemical characteristics of a permanent Spanish hypersaline lake: La Salada de Chiprana (NE Spain). *Hydrobiologia* 267:113–125.

Westall, F. (2008) Morphological biosignatures in terrestrial and extraterrestrial materials. *Space Sci Rev* 135:95–114.

Westall, F. (2011) Early life: nature, distribution and evolution. In *Origins and Evolution of Life: an Astrobiological Perspective*, edited by M. Gargaud, P. López-García, and H. Martin, Cambridge University Press, pp 391–413.

Westall, F. and Cavalazzi, B. (2011) Biosignatures in rocks. In *Encyclopedia of Geobiology*, edited by V. Thiel and J. Reitner, Springer, Berlin, pp 189–201.

Westall, F. and Folk, R.L. (2003) Exogenous carbonaceous microstructures in Early Archean cherts and BIFs from the Isua Greenstone Belt: implications for the search for life in ancient rocks. *Precambrian Res* 126:313–330.

Westall, F., De Wit, M.J., Dann, J., Van Der Gaast., S., De Ronde., C., and Gerneke., D. (2001) Early Archaean fossil bacteria and biofilms in hydrothermally influenced, shallow water sediments, Barberton Greenstone Belt, South Africa. *Precambrian Res* 106:91–112.

Westall, F., de Ronde, C.E.J., Southam, G., Grassineau, N., Colas, M., Cockell, C., and Lammer, H. (2006) Implications of a 3.472–3.333 Gyr-old subaerial microbial mat from the Barberton greenstone belt, South Africa for the UV environmental conditions on the early Earth. *Philos Trans R Soc Lond B Biol Sci* 361:1857–1875.

White, J.F. and Corwin, J.F. (1961) Synthesis and origin of chalcedony. *Am Mineral* 46:112–119.

Address correspondence to:
D. Gourier
Laboratoire de Chimie de la Matière Condensée de Paris
Ecole Nationale Supérieure de Chimie de Paris
UMR CNRS 7574
13 rue Pierre et Marie Curie
75005 Paris
France

E-mail: didier-gourier@chimie-paristech.fr

Submitted 26 March 2012
Accepted 7 November 2012